Bioelectrochemistry 128 (2019) 56–65

Contents lists available at ScienceDirect

Bioelectrochemistry

journal homepage: www.elsevier.com/locate/bioelechem

Towards a dual in-line electrochemical biosensor for the determination of glucose and hydrogen peroxide

Jeyaraman Shankara Narayanan, Gymama Slaughter *

Old Dominion University, Frank Reidy Reseach Center for Bioelectrics, Department of Electrical and Computer Engineering, Virginia, USA

ARTICLE INFO

Article history:
Received 22 December 2018
Received in revised form 18 March 2019
Accepted 18 March 2019
Available online 19 March 2019

Keywords:
Dual-sensing
Biosensor
Gold nano particle
Horseradish peroxidase
Colloidal platinum

ABSTRACT

Herein, we report the development of a sensitive and selective dual mode electrochemical platform for the detection of glucose and H_2O_2. The platform is based on tungsten and gold microwire electrodes decorated with gold nanoparticles (AuNPs) and colloidal platinum (colloidal-Pt), respectively. The nanostructured AuNPs electrode was used as a support matrix for the immobilization of horseradish peroxidase (HRP) and the colloidal-Pt served as the non-enzymatic glucose biosensor in the construction of a dual in-line electrochemical biosensor that provides a microenvironment for HRP and a pathway for analyte diffusion via the high surface area. The dual-mode approach allows for the simultaneous detection of glucose and H_2O_2. The glucose biosensor exhibited a dynamic linear range of 0.5 mM to 8 mM glucose. Linearity for H_2O_2 was up to 70 μM. Operational stability resulted in 75% of the initial biosensor response after 27 days. The dual in-line biosensor showed good sensitivity of 0.403 mA mM^{-1} cm^{-2} for glucose and 0.193 mA mM^{-1} cm^{-2} for H_2O_2 in addition to good anti-interference ability. Thus, the low-cost and simple dual in-line biosensor can be used for the real-time detection of glucose and H_2O_2 in the clinical, biological and environmental fields.

1. Introduction

The presence of elevated glucose and hydrogen peroxide (H_2O_2) undoubtedly plays an important role in tissue inflammation with the capability of damaging several cell types [1–5]. Glucose and H_2O_2 produced by mammalian cells play a key role in mediating diverse physiological responses such as cell proliferation, differentiation, and migration [6]. For example, elevated concentrations of glucose and H_2O_2 in the body are considered as one of the important parameters that represent the different states of disorder [7,8]. Consequently, many types of glucose and hydrogen peroxide sensors have been developed, among which sensors based on the electrochemical principle have been of particular interests due to their irreplaceable properties, such as low detections limit, high selectivity and sensitivity [9–11]. In particular, electrochemical sensors are capable of converting chemical or biological information rapidly, ranging from the concentration of specific analyte to the total composition analysis, into an electrical signal [12–18]. During the past a few decades, electrochemical sensors have continued to attract significant attention because of their unique advantages, such as ease of fabrication, rapid response time, low limit of detection, high selectivity and sensitivity [9,19].

The determination of glucose and H_2O_2 has been widely utilized in clinical and biotechonology industry [14]. Nowadays, there is an increasing trend towards the integration of nanomaterials for electrochemical sensing in order to improve the sensitivity among other properties of the sensor. Most of the biosensors aimed at the detection of various analytes consist of an array of "transducers" immobilized with "receptors" such as enzymes, aptamers or antibodies [9,16]. Materials like carbon nanotubes [20,21], metal oxides [22,23], nano-structured conducting polymers [24–26], graphene [27], graphene-based hybrid materials including graphene quantum dots [28], polyvinylpyrrolidone-protected graphene /polyethylenimine functionalized ionic liquid [29], reduced graphene oxide/PAMAM-silver nanoparticles nanocomposite [30] and reduced graphene oxide-multiwalled carbon nanotubes [31] have been used to construct the transducer. Moreover, particular interest has been shown towards the utilization of noble metals such as gold, platinum and silver nanoparticles/ nanofeatures in general because of their unique electrochemical properties [11,32,33]. These nanoparticles not only improve the direct electron transfer, signal transduction and efficiency of the sensor, but it also provides anchorage for the effective and organized immobilization of enzymes over the surface of the transducer [34–36]. Furthermore, functionalizing the surface of the nanoparticle for enzyme immobilization is an easy one-step process [32]. Platinum nanoparticles have been shown to have the capacity to directly electro-oxidize glucose even in the absence of enzymes and mediators [37]. The large surface area, good biocompatibility of nanoparticles makes nanoparticles and nanocomposites attractive for the construction of biosensor [37–39].

In the present work, a low-cost and simple dual in-line biosensor is developed for the quantitative determination of glucose and H_2O_2 based on colloidal-Pt and HRP/AuNPs electrodes, respectively. The

* Corresponding author.
E-mail address: gslaught@odu.edu (G. Slaughter).

https://doi.org/10.1016/j.bioelechem.2019.03.005
1567-5394/

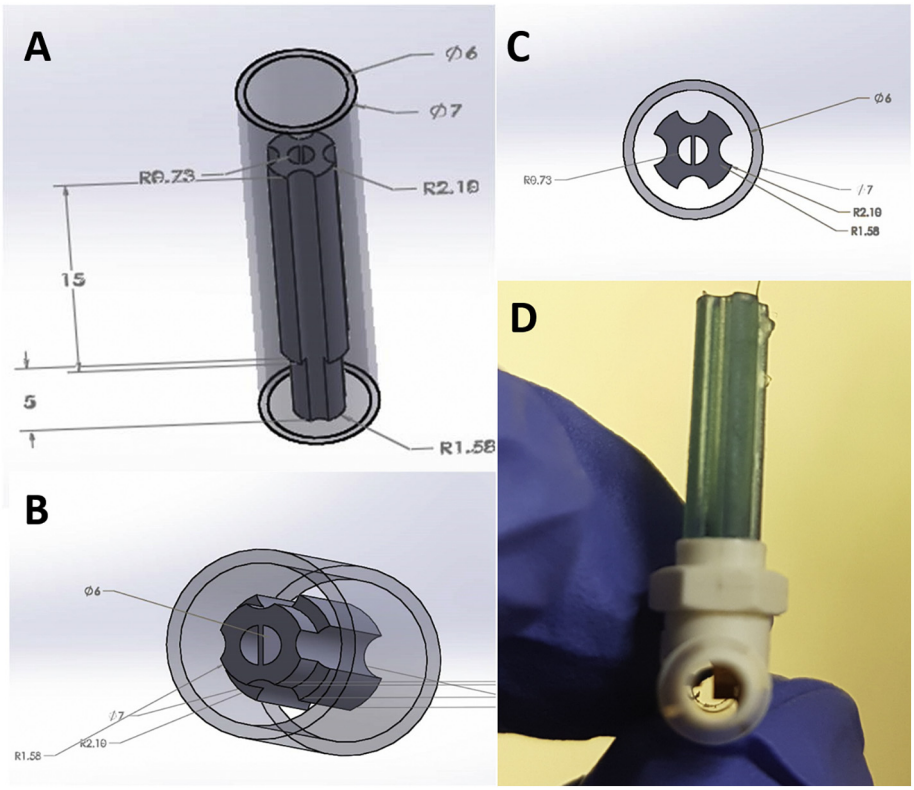

Fig. 1. Solidworks rendering of in-line tube: (A) conceptual drawing of the in-line tube, (B) perspective view, (C) cross sectional view, showing the grooved slots for working electrode and (D) 3D printed in-line tube.

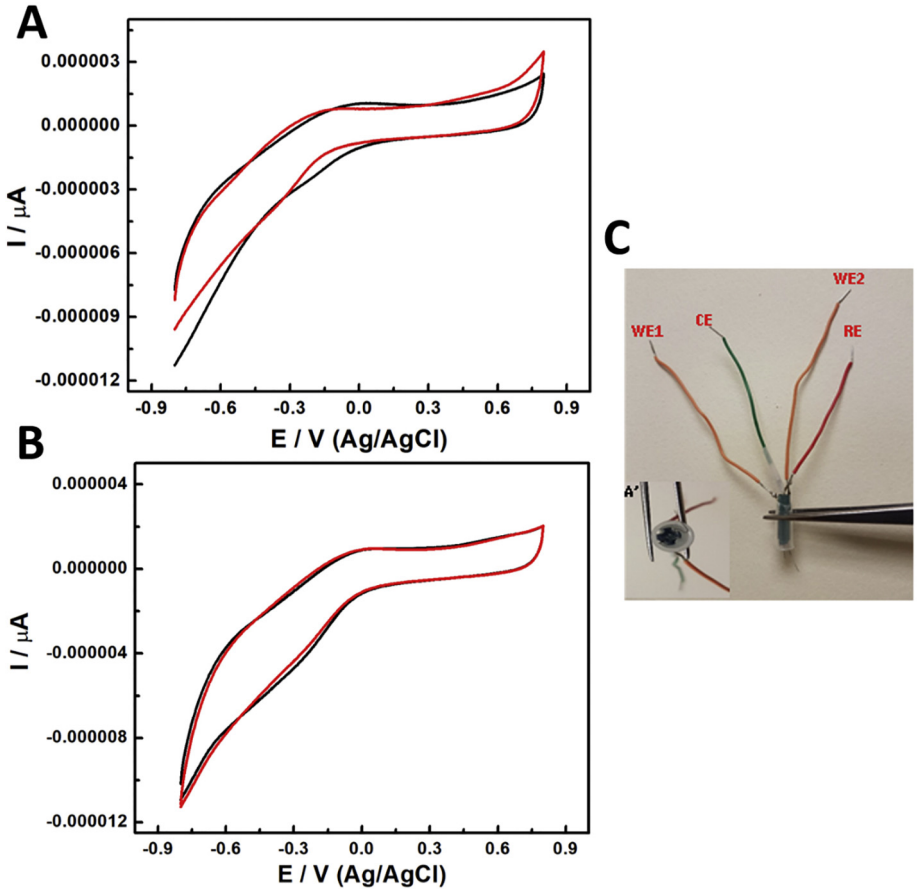

Fig. 2. Cyclic voltammograms recorded in 10 mM phosphate buffer as a supporting electrolyte for (A) As-fabricated Ag/AgCl reference electrode (black curve) and (B) Pt wire electrode (black curve) in 10 mM phosphate buffer solution. Commercially available glassy carbon electrode, Ag/AgCl and Pt wire were used as the working, reference and counter electrodes, respectively. (C) Reference, counter and two working electrodes integrated into the 3D printed in-line tube (Insert: A'- top view).

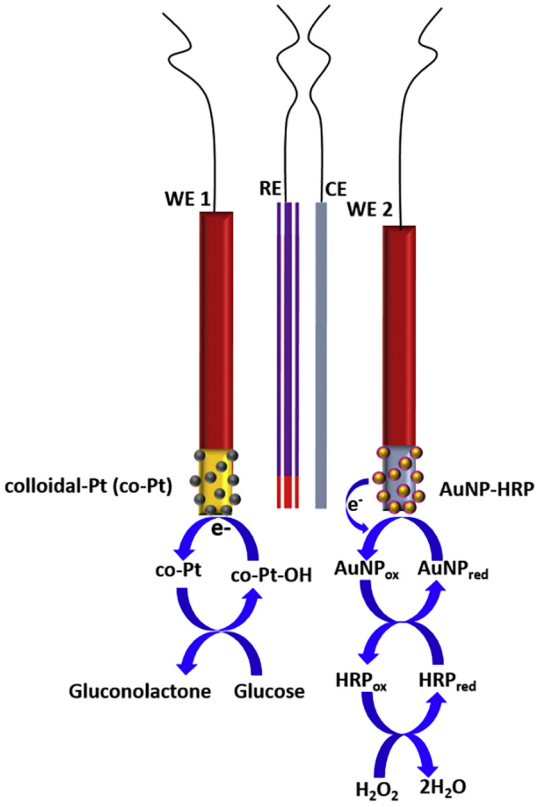

Scheme 1. Schematic representation of the integrated electrode with glucose and H_2O_2 sensing mechanism.

AuNPs served as a support matrix for HRP immobilization and its synthesis was successfully achieved using electrochemical deposition followed by mercaptopropionic acid (MPA) and 1-ethyl-3-(3-dimethylaminopropyl) carbodiimide (EDC) and N-hydroxysuccinimide (NHS) coupling. The analytical performances of the non-enzymatic glucose and enzyme (HRP) electrodes were evaluated simultaneously using cyclic voltammetry (CV) and chronoamperometry (CA). The colloidal-Pt and HRP/AuNPs biosensor showed high sensitivity, good selectivity and stability to the oxidation of glucose and the reduction of H_2O_2, suggesting the dual in-line biosensor strategy can be extended to the development of multimodal biosensors.

2. Materials & methods

2.1. Materials

Glucose, hydrogen peroxide, isopropyl alcohol (IPA), ethanol, sodium hydroxide, horseradish peroxidase (HRP), glycol-chitosan, auric chloride ($HAuCl_4$), silver wire (Ag, 99.9%), platinum wire (Pt, 99.9%), gold wire (Au, 99.99%) and potassium phosphate monobasic were acquired from Sigma-Aldrich (St. Louis, MO). 1-Ethyl-3-(3-dimethylaminopropyl) carbodiimide (EDC) and N-hydroxysuccinimide (NHS) was bought from Pierce Chemical Company (Waltham, MA). Phosphate buffer (PBS) pH 7.4 were prepared with 18.2 MΩ.cm Milli-Q water. The photoreactive Clear Resin L1 comprise methacrylated oligomers and methacrylated monomer and photoinitiator and was acquired from Formlabs (Somerville, MA).

2.2. Electrochemical measurements

Electrochemical measurements of the cyclic voltammetry (CV) and chronoamperometry (CA) were performed with a BASi-Epsilon electrochemical workstation (BASi, Indiana, USA), using the setup of a four-electrode electrochemical configuration, with the modified colloidal-Pt and HRP/AuNPs as the dual in-line working electrodes, and platinum wire and as-fabricated Ag/AgCl electrodes as the counter and reference electrodes, respectively. Electrochemical measurements were conducted in a sample volume of 200 μl electrolyte solution comprising 0.5 mM to 13 mM glucose and 0.5 μM to 70 μM H_2O_2, which are the concentration levels typically observed in tissue inflammation. All electrochemical experiments were carried out at room temperature. The collection of blood samples from diabetic subjects have been previously reported [40], wherein the extracted plasma was flash frozen in −70 °C freezer until used. Plasma glucose concentrations varied from 2.77 mM, 4.99 mM to 9.99 mM and were measured using a glucose analyzer (Beckman, Fullerton, CA). The corresponding plasma glucose solution was further spiked with H_2O_2 to obtain 10 μM, 25 μM H_2O_2 to 50 μM H_2O_2.

2.3. Design of the in-line tubing

The 3D printing process was carried out in a stereolithography (SLA) 3D printer (Form 2 SLA 3D Printer, Formlabs, Massachusetts, USA) and the printing geometries were designed in Solidworks 2018 × 64 Editor. Typically the printing of the samples was performed at a temperature of 35 °C with 50 μm of resolution. Basic 2D renderings and extrusions were used to designed the in-line tubing in SolidWorks to house the electrodes. The length of the in-line tube is 15 mm with two 0.7 mm half-hollowed cores in the inner tubing to house the common reference and counter electrodes. Four grooves with a radius of 2.1 mm are incorporated to hold up to four working electrodes (Fig. 1A and B). A cross sectional view of the designed in-line tube is shown in Fig. 1C, where the outer tubing secures the electrodes mounted on the inner tubing in place. Working electrodes can be easily mounted in north, east, west and south side of the inner tube, while the reference and counter electrodes reside separately in the half-hallowed cores. The 3D data from SolidWorks were acquired with FormLabs 3D printer and converted to .stl file, which was necessary for the 3D printer. The Form2 stereolithographic printer was used to produce prints at 50 μm

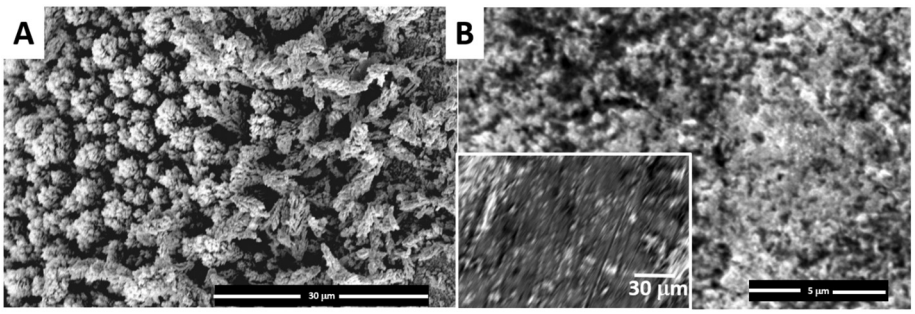

Fig. 3. SEM images of (A) electrodeposition of Colloidal-Pt on gold microwire and (B) magnified image of horseradish peroxidase (HRP) immobilized on electrodeposited AuNPs via MPA. (For interpretation of the references to colour in this figure legend, the reader is referred to the web version of this article.)

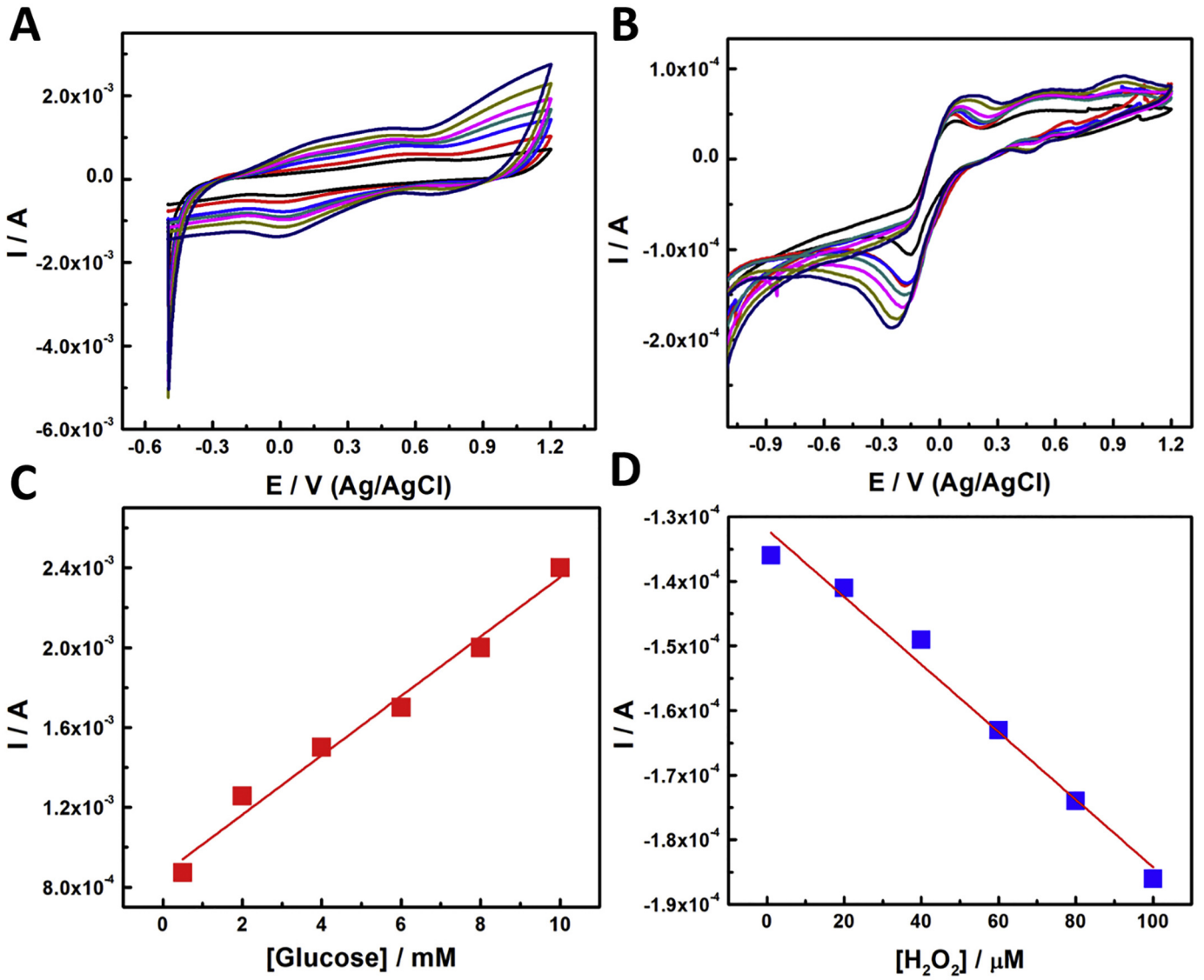

Fig. 4. Simultaneous cyclic voltammagrams of dual in-line sensor in the absence (curves a) and in the presence (curves b–g) of A) glucose (0.5 mM–10 mM) and B) H_2O_2 (1 µM–100 µM). Linear dependence of C) glucose and D) H_2O_2 current response obtained from cyclic voltammetry.

resolution with clear resin. The printed parts were post-processed with two isopropyl alcohol washes followed by UV curing to realize the final 3D part rendered in Fig. 1D.

3. Reference and counter electrodes fabrication

A 20 mm long and 1 mm thick silver (Ag) wire is immersed briefly in 0.1 M HNO_3 to remove any oxide layer formed on the surface of the Ag wire and immediately rinsed with DI water, IPA and dried in a stream of N_2 gas. The Ag wire electrode is then oxidized in an electrolyte containing 3 M NaCl at $^{+}$700 mV applied potential using CA technique to form a grayish-white coating of AgCl on the surface of the Ag wire. The fabricated Ag/AgCl reference electrode is then rinsed and stored in 3 M KCL for further use. A 20 mm long platinum wire ($\phi = 0.5$ mm) was used as a counter electrode. The as-fabricated Ag/AgCl electrode and a commercially available Ag/AgCl reference electrode were evaluated in 3 M KCl. The electrode potential, was measured by a multimeter in order to calibrate the as-fabricated Ag/AgCl electrode potential. The potential was 0.018 V versus the commercial Ag/AgCl electrode. In addition, the performance of the Ag/AgCl reference electrode was examined by cyclic voltammetry in 10 mM phosphate buffer solution using three-electrode configuration, a commercial glassy carbon working and Pt counter electrodes. A very good correlation was observed between the CVs with the as-fabricated Ag/AgCl electrode and the commercially available Ag/AgCl reference electrode as shown in Fig. 2A. The CV curve for the as-fabricated reference electrode showed an increase in the oxidation current compared to commercial Ag/AgCl, which is within the experimental error. In addition, no significant potential differences were observed. The Pt wire counter electrode was also examined versus commercially available Pt electrode from BASi. The CV profiles were identical as shown in Fig. 2B. Overall, the potential and peak current profile for both the as-fabricated Ag/AgCl and Pt wire electrode remained constant for multiple numbers of cycles, thereby signifying a stable Ag/AgCl and Pt electrode [41]. Afterwards, all the electrodes are soldered to electrical wire leads to enable easy handling and interrogation by the electrochemical workstation (Fig. 2C). The electrodes are then inserted into the electrolyte comprising of glucose and H_2O_2 for further electrochemical characterizations.

3.1. Working electrodes fabrication

Colloidal-Pt was electroideposited onto the surface of Au wire ($l =$ 20 mm $\phi = 0.5$ mm) using a three-electrode configuration in YSI 3140 platinizing solution, where Pt wire and Ag/AgCl electrodes served

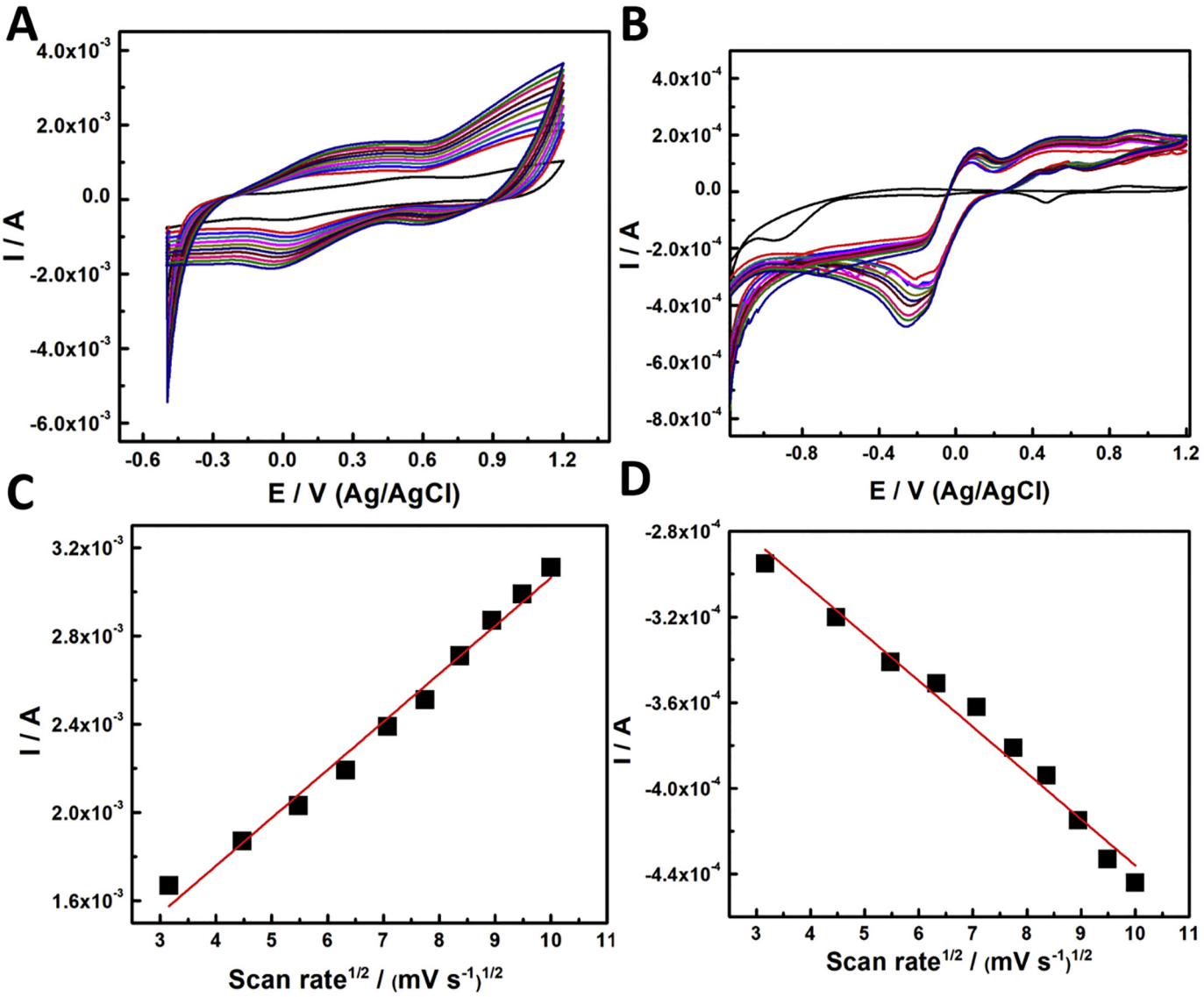

Fig. 5. Cyclic voltammograms obtained by A) Collodial-Pt electrode in the presence of 5 mM glucose and B) HRP/AuNPs electrode in the presence of 25 μM H_2O_2. Scan rate range 10–100 mV s^{-1}. C & D) Plot of Ip versus $v^{1/2}$.

as the counter and reference electrodes, respectively. A potential of −225 mV was applied for 1500 s followed by DI rinsed to remove loosely bound colloidal-Pt. The colloidal-Pt coated Au wire was baked at a temperature of 260 °C for 5 min to improve solidity of the platinum coating at the surface of the Au wire. The electrode surface is then coated with 1% glycol chitosan to enhance the device selectivity towards glucose. Tungsten wire (l = 20 mm ϕ = 0.2 mm) was cleaned with IPA, ethanol and dried in a stream of N_2 gas followed by electrodeposition AuNPs from 1 mM $HAuCl_4 \cdot nH_2O$ solution at −0.2 V (vs. Ag/AgCl) for 50 s. The AuNPs electrode was incubated in 1 mM mercaptopropionic acid (MPA) in phosphate buffer solution for 1 h. The thiol tail group of MPA self-assembles on the surface of the AuNPs by forming a strong covalent bond between the thiol group and gold. After surface functionalization, the AuNPs electrode was washed with buffer to remove any unbound MPA. The carboxylic acid head group of MPA was then activated by 0.8 mg EDC and 2.2 mg NHS along with 1 mg of HRP in 100 mM PBS 7.4 overnight at 4 °C. In presence of the EDC, the N-hydroxyl group of the NHS interacts with the carboxyl groups to form reactive sites, where the amino group of HRP displaces the succinimide group of NHS to form a peptide bond. The surface area of the HRP modified electrode is calculated to be 0.0314 cm^2 using the geometric area. The schematic representation of the fabricated electrode with their respective reaction mechanism is shown in Scheme 1.

4. Results and discussion

4.1. Characterization of colloidal-Pt and HRP/AuNPs

An SEM image of the as fabricated colloidal-Pt and HRP/AuNPs electrode structures as mentioned in the working electrodes fabrication is shown in Fig. 3A and B, respectively. In the case of electrodeposition of colloidal-Pt, the SEM result shows aggregated micron size cluster rod-like morphology over the gold microwire surface (Fig. 3A). The colloidal-Pt is composed of particles with diameter in the range of 300–450 nm and length of a few micrometers as seen in the Fig. 3A. In addition, the colloidal-Pt exhibited irregular spheroidal and rod-like morphologies, which are built with nanowires forming a hierarchical micro/nanostructure. The SEM images of AuNPs and AuNPs modified with HRP are also shown to depict the immobilization of HRP on the surface of AuNPs. The morphology of the electrodeposited AuNPs is depicted in Fig. 3B insert. One can see that the AuNPs coated the surface of the tungsten microwire and the surface becomes rough. The tungsten

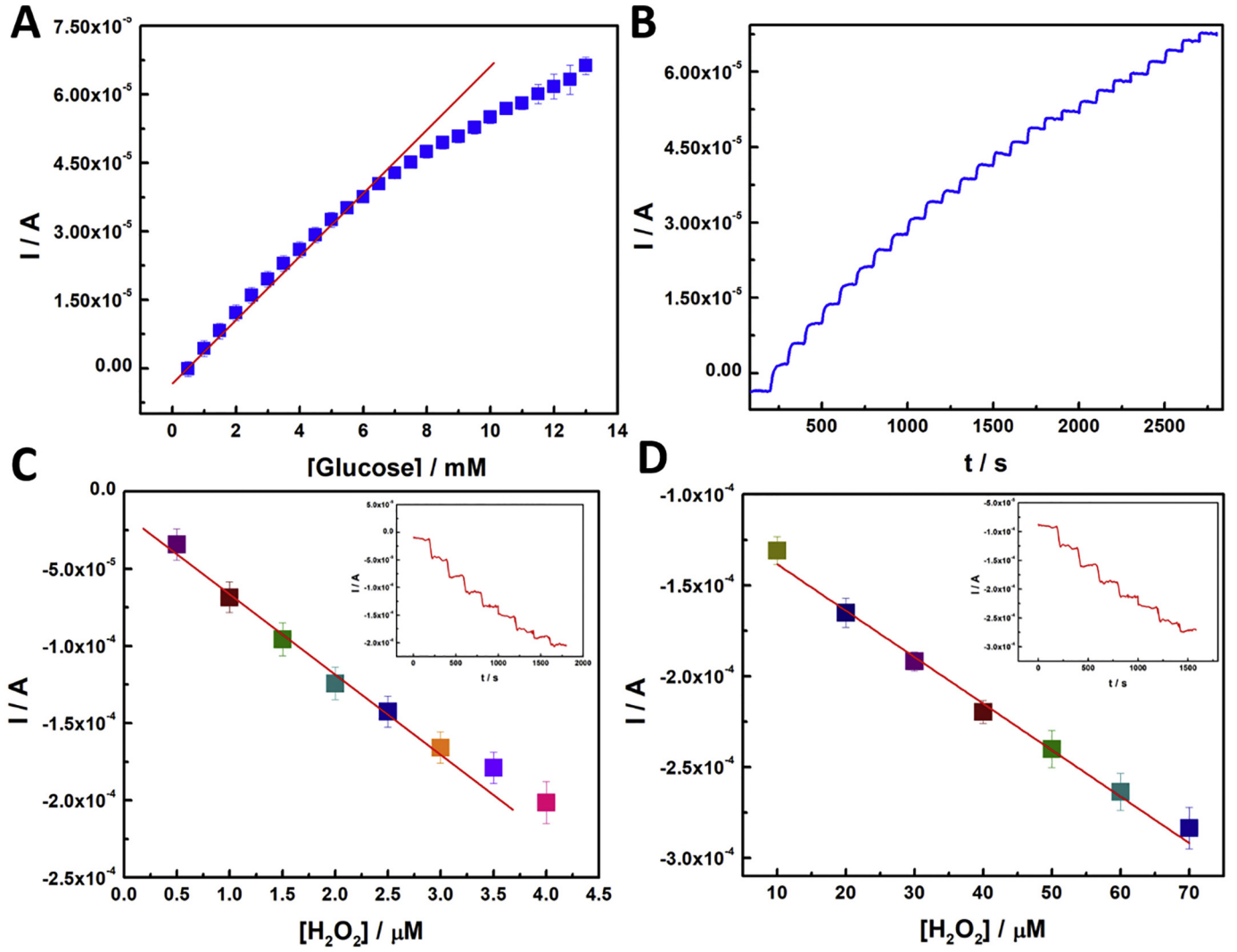

Fig. 6. (A, C–D) Calibration curve for glucose and H_2O_2 measurement (Insets C–D) Current-time response observed with colloidal-Pt and HRP/AuNPs to successive addition of a mixture containing glucose and H_2O_2 in 10 mM phosphate buffer (pH 7.4). -100 mV applied was applied to both working electrodes.

microwire surface showed the presence of HRP after covalent immobilization with mean diameter of ~200 nm as seen in Fig. 3B. The HRP enzymes completely covered the surface of the AuNPs electrode. This

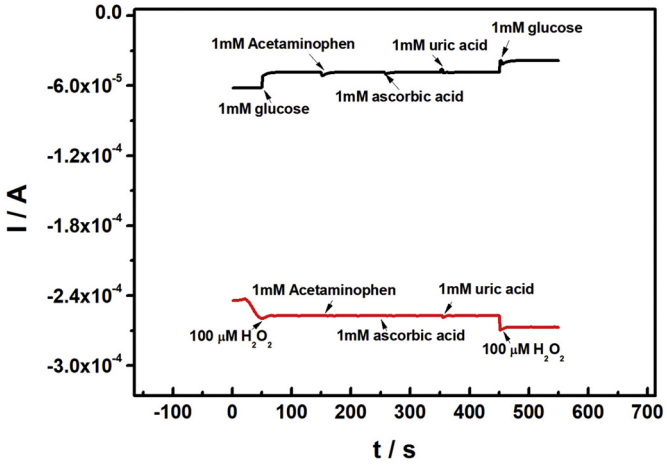

Fig. 7. Selectivity behavior of the dual in-line electrochemical biosensor examined in the presence of common interferring species such as acetaminophen, ascorbic acid and uric acid.

covalent immobilization of HRP is useful in order to avoid desorption of the enzymes during repeated successive usage.

4.2. Dual electrochemical behavior of colloidal-Pt and HRP/AuNPs

The electrochemical behavior of the dual in-line colloidal-Pt and HRP/AuNPs towards the oxidation of glucose and reduction of H_2O_2 is studied by cyclic voltammetry. Fig. 4 shows the cyclic voltammetry response of colloidal-Pt (Fig. 4A) and HRP/AuNPs (Fig. 4B) recorded simultaneously in 10 mM phosphate buffer solution (pH 7.4) and in the presence of the electrolyte mixture containing various concentrations of glucose and H_2O_2 in a potential window of −1.2 to +1.2 V recorded at 50 mV s^{-1} via a bi-potentiostat. Fig. 4A curve 'a' shows the electrode response in 10 mM phosphate buffer solution and curve 'b' through 'g' shows the respective response in the presence of increasing glucose concentrations (0.5 mM – 10 mM). The CV response of the colloidal-Pt modified electrode exhibited a stable and broadly-defined oxidation peak corresponding to glucose oxidation at +400 mV with an onset potential at ca.-200 mV, which is comparable to the oxidation of glucose to glucolactone catalyzed by the Pt nanoparticles observed by Ciu et al. [42]. In the presence of glucose, a negative shift of the anodic peak potential and a substantial increase of current signal was observed in the presence of increasing glucose concentrations. It can also be observed that the HRP/AuNPs electrode (Fig. 4B) presented a well-defined reduction peak

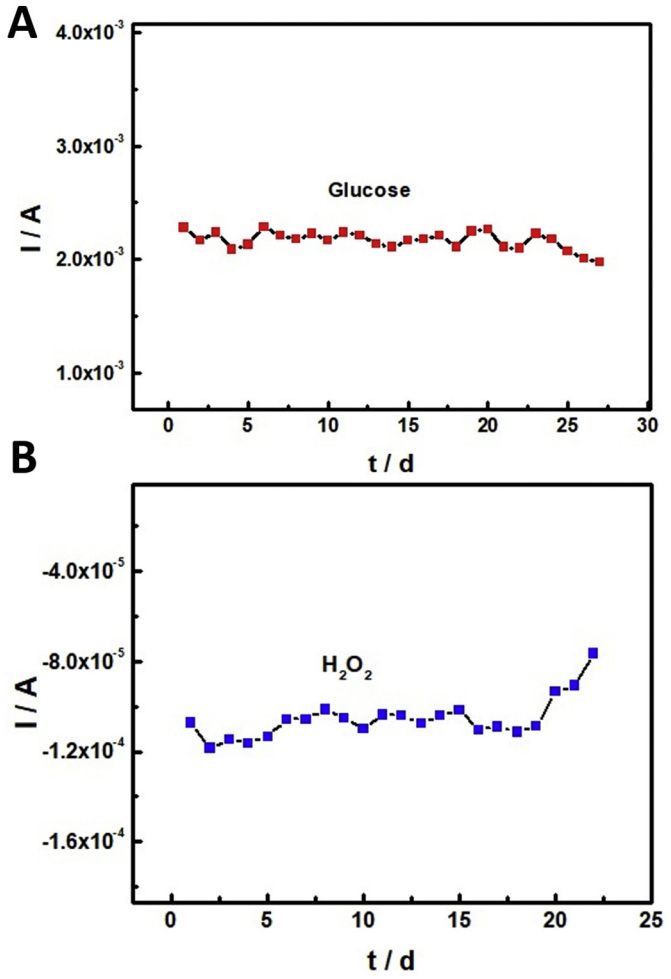

Fig. 8. Stability of the colloidal-Pt and HRP/AuNPs dual in-line electrodes examined for 27 consecutive days after the addition of mixture of 1 mM glucose and 100 μM H_2O_2. (A) Colloidal-Pt and (B) HRP/AuNPs current-time response. Electrodes were stored in 10 mM PBS after every successive day of measurement.

for H_2O_2 at ca. −200 mV, which is comparable to those previously reported [11,43]. In the presence of increasing H_2O_2 (1 μM–100 μM) concentrations, the reduction current signals were observed to significantly increased. Thereby indicating that the electron transfer mechanism may involve the participation of both HRP and AuNPs and AuNPs may act as an electron mediator. The above results indicate that the immobilization of HRP on the surface of AuNPs improved the electrocatalytic activity towards the reduction of H_2O_2. The electrodeposition of colloidal-Pt and AuNPs on microwire electrodes takes advantage of the electrocatalytic activity and high surface area of both colloidal-Pt and AuNPs, and provides an easy way to prepare nanostructured electrodes. Furthermore, the CV studies showed that in a mixture of glucose and H_2O_2, distinct peaks can be observed for each analyte, clearly demonstrating the ability of each electrode to discriminate one analyte from the other.

The influence of scan rate on the current response for the anodic current (Ipa) of glucose oxidation and cathodic current (Ipc) of H_2O_2 was also studied. Fig. 5 shows the redox behavior of the colloidal-Pt and HRP/AuNPs electrodes in phosphate buffer solution in the presence of 5 mM glucose and 25 μM H_2O_2 at different scan rates (10 mV s^{-1} to 100 mV s^{-1}). At both colloidal-Pt and HRP/AuNPs electrodes, the currents of the corresponding oxidation and reduction peaks increased with the increase of scan rate. As shown in Fig. 5, the peak currents for glucose H_2O_2 show linear dependence on the square root of the scan rate ($R = 0.986$ and $R = 0.977$), respectively and follows the Randles–Sevcik equation $i_p = 0.463\, nFAC\, (\frac{nFvD}{RT})^{\frac{1}{2}}$. In this equation, i_p is the maximum current, n is the number of electron transfer, F is Faraday constant (C mol^{-1}), A is the electrode area (cm^2), C is concentration in mol cm^{-3}, R is the gas constant (8.314 Jmol^{-1} K^{-1}), T is the room temperature (298.15 K in this case), D is the diffusion coefficient (cm^2 s^{-1}), and v is the scan rate (V s^{-1}). The linear correlation between the catalytic current and square root of the scan rate can be used to obtain the apparent diffusion coefficient, D of the colloidal-Pt and HRP/AuNPs modified electrode, thereby indicating a surface controlled process.

4.3. Amperometry

Quantification of glucose and H_2O_2 was carried out by acquiring the chronoamperograms of the colloidal-Pt and HRP/AuNPs in a stirring 10 mM phosphate buffer supporting electrolyte followed by successive addition of glucose and H_2O_2 aliquots at the operating potential of −100 mV, which resulted in the maximum oxidation and reduction currents, respectively. Fig. 6 depicts the amperograms showing the addition of the aliquot solutions. The oxidation current increased almost instantaneously to a steady state oxidation current within 3 s upon the addition of the glucose and H_2O_2 aliquots (Fig. 6A and C), thereby reflecting the sensitive response of the colloidal-Pt to glucose in the dual in-line biosensor (Fig. 6C). At the same time, a steep increased in the reduction current was observed at the HRP/AuNPs for H_2O_2 (Fig. 6B, D). The fast sensor response observed is attributed to the catalytic activity on the colloidal-Pt and HRP/AuNPs, wherein electrons are directly transferred to the electrode surface. The calibration curves were constructed by plotting the steady-state current as a function of glucose and H_2O_2 concentrations. The calibration plots exhibit a linear behavior over the concentration range of 0.5 mM to 8 mM glucose ($r^2 = 0.984$) and 0.5 μM to 70 μM ($r^2 = 0.987$) for glucose and H_2O_2, respectively. The detection limit was calculated using 3σ/S, where σ and S is the blank standard deviation and sensitivity, respectively and was found to be 430 μM for glucose and 0.41 μM H_2O_2, which exhibits enhanced detection limit than those reported for hydrogen peroxide over the gold and silver nanocomposite electrode [44,45]. In addition, the biosensor exhibited high sensitivity of 0.403 mA mM^{-1} cm^2 towards glucose and 0.193 mA mM^{-1} cm^2 towards H_2O_2. The excellent sensitivity of the biosensor indicates that there is a good degree of efficiency associated with the electrodeposition of colloida-Pt and the immobilization of HRP and AuNPs.

The dual in-line biosensor demonstrated an extended linear dynamic range, operational stability and good sensitivity when compared to other dual glucose and H_2O_2 biosensors [45-47]. The glucose linear range achieved in previous studies are not in physiological glucose or H_2O_2 range [46,47], thereby limiting their application in glucose and H_2O_2 determination in biological samples. Although the work by Krishnan et al. [47] covered the physiological glucose range (1–12 mM), the H_2O_2 range is well above the physiologic level (1–5 mM).

4.4. The effect of interfering species

To demonstrate the selectivity of the fabricated electrodes for dual glucose and H_2O_2 detection, a few common interferents were examined. Fig. 7 shows the amperometric response towards the addition of a solution comprising 1 mM glucose and 100 μM H_2O_2 followed by 1 mM acetaminophen, ascorbic acid and uric acid injections. There were no noteworthy amperometric responses observed when compared to the response current of the biosensor in the presence of 1 mM glucose and 100 μM H_2O_2. The interferents examined did not exhibit any significant response of the dual in-line biosensor. The enhanced selectivity may be attributed due to the chitosan layer over the colloidal-Pt electrode [48,49] and the HRP/AuNPs electrode. In addition, the applied potential (−100 mV) is not as conducive to the oxidation or reduction of the interfering species and thereby increases the selectivity in the presence of the interfering electroactive species.

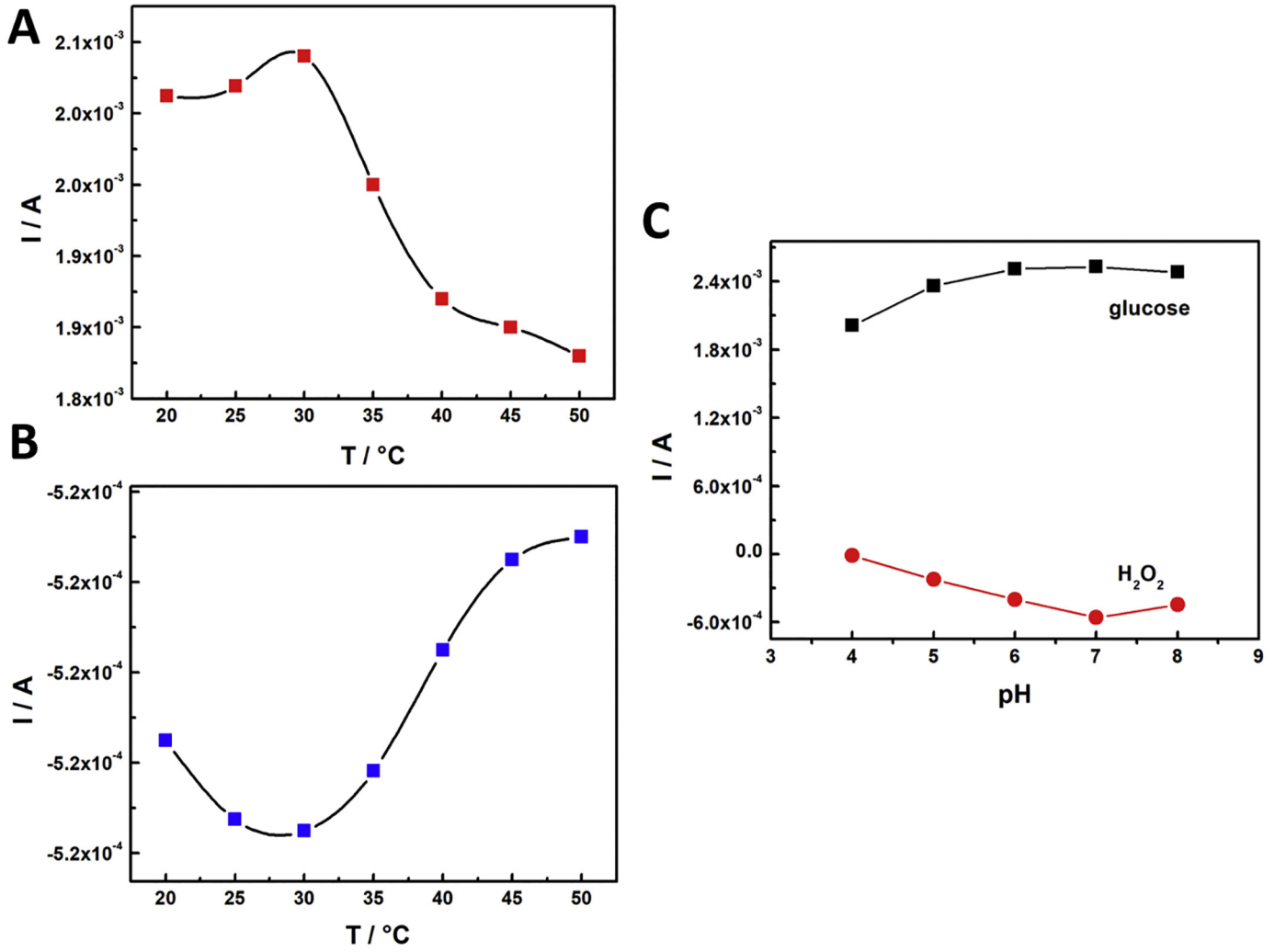

Fig. 9. Temperature (A-B) and pH (C) dependence on colloidal-Pt and HRP/AuNPs microwire electrode in the presence of 5 mM glucose and 25 μM H_2O_2.

4.5. Electrode stability

The operational stability of the fabricated dual in-line biosensor was examined by monitoring the oxidation and reduction current response of colloidal-Pt and HRP/AuNPs at −400 mV for the oxidation and reduction of glucose and H_2O_2. The performance of the electrodes was tested in 1 mM glucose and 100 μM H_2O_2 daily for a period of 27 days. Both the colloidal-Pt and HRP/AuNPs electrodes retained over 75% of their initial current response as shown in Fig. 8. The dual in-line biosensor proved to be stable and allowed the biosensor to be used for a period of 27 days without significant loss of colloidal-Pt and immobilized HRP activity. This is attributed to the robust nature of the glycol chitosan favourable microenviroment and the covalent immobilization of the enzyme to AuNPs to enable the biosensor to exhibit very good stability.

Since the catalytic activity of biosensors relies on different parameters, a pH and temperature profile characterization was performed to determine the working pH and temperature range. Fig. 9 shows that the optimal working temperature of the colloidal-Pt and HRP/AuNPs microwire electrode operating at a fixed pH of 7.4 is 30 °C and the optimal working pH at room temperature is observed to be 7 for both electrodes (Fig. 9C).

It is apparent that the reaction rates increase with temperature, up to 30 °C and beyond this point there may be an irreversible thermal degradation in HRP and colloidal-Pt. The working temperature range for colloidal-Pt is between 20 °C and 30 °C, while for HRP/AuNPs, the range is slightly higher, up to 35 °C. Importantly, both electrode exhibited a working pH range between 6 and 8, wherein the dual in-line biosensor responses are observed to be reproducible and show good sensitivity when operating outside optimum conditions.

In addition, the fabricated dual in-line biosensor exhibited good response activity for the determination of glucose and H_2O_2 in blood plasma (Fig. 10). The colloidal-Pt electrode exhibited a sensitivity of 0.0314 mA mM^{-1} cm^{-2} for the concentration range of 2.7 mM to 9.9 mM glucose, while the HRP/AuNPs electrode exhibited a higher sensitivity of 7.81 mA mM^{-1} cm^{-2} for the concentration range of 10 μM to 50 μM H_2O_2. The difference in sensitivity is attributed to the accumulation of protein in the extracted blood plasma and protein adhesion on the surface of the biosensor, thereby, limiting the diffusion of the biomolecules to the surface of the sensor. This results shows that the dual in-line biosensor can monitor glucose and H_2O_2 in biological samples.

5. Conclusion

A dual in-line biosensor for the ultrasensitive detection of glucose and hydrogen peroxide has been successfully fabricated based on colloidal-Pt and HRP/AuNPs, respectively. The electrodeposited AuNPs served as a supporting nanomatrix for HRP immobilization via MPA self-assembly and EDC/NHS coupling to result in a stable biosensor. The sensor exhibited an excellent detection limit of 430 μM and 0.41 μM for both glucose and hydrogen peroxide, respectively. The dual in-

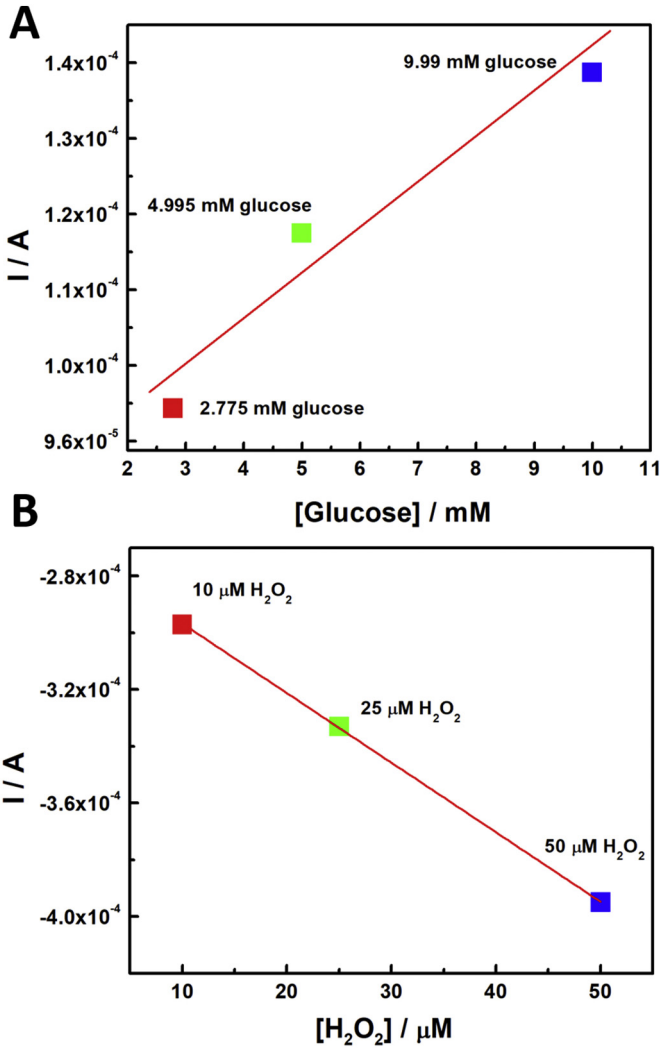

Fig. 10. Dual in-line biosensor amperometric response to glucose (A) and (B) H_2O_2 in blood plasma.

line biosensor exhibits a detection sensitivity of 0.403 mA mM^{-1} cm^{-2} for glucose and 0.193 mA mM^{-1} cm^{-2} for H_2O_2. The sensor showed remarkable selectivity in the presence of common interfering species due to the lower operating potential. The dual in-line biosensor showed high operational stability with a good linear dynamic range. Furthermore, the result indicates the biosensor can simultaneous and continuous detect glucose and H_2O_2, which has practical applications in clinincal and food industries.

Acknowledgements

This work was supported by Department of Defense, Department of the Army, United States Army Medical Command and Materials Research (USAMCMR Award W81XWH-17-1-0452). The authors thank the Keith Porter Imaging Facility (KPIF) at the University of Maryland Baltimore County (UMBC) for providing the 3D printing services.

References

[1] T.V. Kirk, M.P.C. Marques, A.N.P. Radhakrishnan, N. Szita, Quantification of theoxygen uptake rate in a dissolved oxygen controlled oscillating jet-driven microbioreactor, J. Chem. Technol. Biotechnol. 91 (2016) 823–831.
[2] J. Ehgartner, P. Sulzer, T. Burger, A. Kasjanow, D. Bouwes, U. Krühne, Online analysis of oxygen inside silicon-glass microreactors with integrated optical sensors, Sens. Actuators B Chem. 228 (2016) 748–757.
[3] N. Deepa, A.B. Ganesh, Minimally invasive fluorescence sensing system forreal-time monitoring of bacterial cell cultivation, Instrum. Sci. Technol. 45 (2017) 85–100.
[4] B. Ungerbock, V. Charwat, P. Ertl, T. Mayr, Microfluidic oxygen imaging using integrated optical sensor layers and a color camera, Lab Chip 13 (2013) 1593–1601.
[5] A. Shamirian, H. Samareh Afsari, A. Hassan, L.W. Miller, P.T. Snee, In-vitro detection of hypoxia using a ratio metric quantum dot-based oxygen sensor, ACS Sensors 1 (2016) 1244–1250.
[6] Z.H. Wang, J.B. Yu, R.J. Gui, H. Jin, Y.Z. Xia, Carbon nanomaterials-based electrochemical aptasensors, Biosens. Bioelectron. 79 (2016) 136–149.
[7] S.S. Mahshid, S. Camire, F. Ricci, A. Vallee-Belisle, A highly selective electrochemical DNA-based sensor that employs steric hindrance effects to detect proteins directly in whole blood, J. Am. Chem. Soc. 137 (2015) 15596–15599.
[8] S. Jeong, J. Park, D. Pathania, C.M. Castro, R. Weissleder, H. Lee, Integrated magneto−electrochemical sensor for exosome analysis, ACS Nano 10 (2016) 1802–1809.
[9] G. Slaughter, Current Advances in biosensor design and fabrication, in: R.A. Meyers (Ed.), Encyclopedia of Analytical Chemistry, John Wiley, Chichester, June 14 2018https://doi.org/10.1002/9780470027318.a0505.pub2.
[10] T. Kulkarni, G. Slaughter, Characteristics of two self-powered glucose biosensors, IEEE Sensors J. 17 (2017) 3607–3612.
[11] J.S. Narayanan, G. Slaughter, The preparation of AuNPs-HRP needle-type biosensor for ultrasensitive detection of hydrogen peroxide, Med. Devices Sens. 1 (2018) 1–9.
[12] E. Bakker, Electrochemical sensors, Anal. Chem. 76 (2004) 3285–3298.
[13] D.R. Thevenot, K. Toth, R.A. Durst, G.S. Wilson, Electrochemical biosensors: recommended definitions and classification, Biosens. Bioelectron. 16 (2001) 121–131.
[14] O. Junichi, I. Masahiko, O. Susumu, T. Shinjiro, A. Misato, M. Sawa, T. Masahiro, T. Ayumi, Spectrophotometric determination of hydrogen peroxide, glucose, uric acid, and cholesterol using peroxidase-like activity of an Fe(III) complex of thiacalix[4] arenetetrasulfonate attached to an anion-exchanger, Anal. Sci. 29 (2013) 1041–1048.
[15] X.B. Lu, Z.H. Wen, J.H. Li, Hydroxyl-containing antimony oxide bromide nanorods combined with chitosan for biosensors, Biomaterials 27 (2006) 5740–5747.
[16] D. Chen, H.B. Feng, J.H. Li, Graphene oxide: preparation, functionalization, and electrochemical applications, Chem. Rev. 112 (2012) 6027–6053.
[17] L.H. Tang, Y. Wang, Y.M. Li, H.B. Feng, J. Lu, J.H. Li, Preparation structure and electrochemical properties of reduced graphene sheet films, Adv. Funct. Mater. 19 (2009) 2782–2789.
[18] H.B. Wang, H.D. Zhang, Y. Chen, Y. Li, T. Gan, H_2O_2-mediated fluorescence quenching of double stranded DNA templated copper nanoparticles for label-free and sensitive detection of glucose, RSC Adv. 5 (2015) 77906–77912.
[19] L. Wang, J. Zheng, Y. Li, S. Yang, C. Liu, Y. Xiao, J. Li, Z. Cao, R. Yang, AgNP-DNA@GQDs hybrid: new approach for sensitive detection of H_2O_2 and glucose via simultaneous AgNP etching and DNA cleavage, Anal. Chem. 86 (2014) 12348–12354.
[20] G. Slaughter, Fabrication of Nano-indented-electrodes for glucose detection, J. Diab. Sci. Technol. 4 (2) (2010) 320–327.
[21] D. Ivnitski, K. Artyushkova, P. Atanassov, Surface characterization and direct electrochemistry of redox copper centers of bilirubin oxidase from fungi Myrothecium verrucaria, Bioelectrochemistry 74 (2008) 101–110.
[22] B. Haghighi, B. Karimi, M. Tavahodi, H. Behzadneia, Electrochemical behavior of glucose oxidase immobilized on Pd-nanoparticles decorated ionic liquid derived fibrillated mesoporous carbon, Electroanal. 26 (2014) 2010–2016.
[23] G. Slaughter, J. Sunday, Fabrication of enzymatic glucose hydrogel biosensor based on hydrothermally grown ZnO nanoclusters, IEEE Sensors J. 14 (2014) 1573–1576.
[24] Z. Wang, S. Liu, P. Wu, C. Cai, Detection of glucose based on direct electron transfer reaction of glucose oxidase immobilized on highly ordered polyaniline nanotubes, Anal. Chem. 81 (2009) 1638–1645.
[25] C.X. Guo, C.M. Li, Direct electron transfer of glucose oxidase and biosensing of glucose on hollow sphere-nanostructured conducting polymer/metal oxide composite, Physical. Chem. Chem. Phy. 12 (2010) 12153–12159.
[26] S.I. Brahim, G. Slaughter, A. Guiseppi-Elie, Electrical and electrochemical characterization of electroconductive PPy-p(HEMA) composite hydrogels, Smart Struct. Mat. 5053 (2003) 1–12.
[27] B. Liang, L. Fang, G. Yang, Y. Hu, X. Guo, X. Ye, Direct electron transfer glucose biosensor based on glucose oxidase self-assembled on electrochemically reduced carboxyl graphene, Biosens. Bioelectron. 43 (2013) 131–136.
[28] H. Razmi, R. Mohammad-Rezaei, Graphene quantum dots as a new substrate for immobilization and direct electrochemistry of glucose oxidase: application to sensitive glucose determination, Biosens. Bioelectron. 41 (2013) 498–504.
[29] C. Shan, H. Yang, J. Song, D. Han, A. Ivaska, L. Niu, Direct electrochemistry of glucose oxidase and biosensing for glucose based on graphene, Anal. Chem. 81 (2009) 2378–2382.
[30] Z. Luo, L. Yuwen, Y. Han, J. Tian, X. Zhu, L. Weng, L. Wang, Reduced graphene oxide/PAMAM-silver nanoparticles nanocomposite modified electrode for direct electrochemistry of glucose oxidase and glucose sensing, Biosens. Bioelectron. 36 (2012) 179–185.
[31] V. Mani, B. Devadas, S.M. Chen, Direct electrochemistry of glucose oxidase at electrochemically reduced graphene oxide-multiwalled carbon nanotubes hybrid material modified electrode for glucose biosensor, Biosens. Bioelectron. 41 (2013) 309–315.
[32] P. Yang, L. Wang, Q. Wu, Z. Chen, X. Lin, A method for determination of glucose by an amperometric bienzyme biosensor based on silver nanocubes modified Au electrode, Sensors Actuators B Chem. 194 (2014) 71–78.
[33] X. Che, R. Yuan, Y. Chai, J. Li, Z. Song, W. Li, X. Zhong, A glucose biosensor based on chitosan-Prussian blue-multiwall carbon nanotubes-hollow PtCo nanochains formed by one-step electrodeposition, Colloids Surf. B: Biointerfaces 84 (2011) 454–461.
[34] L. Ruiyi, Z. Juanjuan, W. Zhouping, L. Zaijun, L. Junkang, G. Zhiguo, W. Guangli, Novel graphene-gold nanohybrid with excellent electrocatalytic performance for the electrochemical detection of glucose, Sensors Actuators B Chem. 208 (2015) 421–428.
[35] G. Slaughter, T. Kulkarni, Highly selective and sensitive self-powered glucose sensor based on capacitor circuit, Nat. Sci. Rep. 7 (2017), 1471.

[36] N. Germana, A. Ramanavicius, A. Ramanaviciene, Electrochemical deposition of gold nanoparticles on graphite rod for glucose biosensing, Sensors Actuators B Chem. 203 (2014) 25–34.
[37] Md.Q. Hasan, R. Kuis, J. Shankara Narayanan, G. Slaughter, Fabrication of highly effective hybrid biofuel cell based on integral colloidal platinum and bilirubin oxidase on gold support, Nat. Sci. Rep. 8 (2018), 16351.
[38] J. Zhang, J. Li, F. Yang, B. Zhang, X. Yang, Pt nanoparticles assisted electroless deposition of prussian blue on the electrode: detection of H_2O_2 with tunable sensitivity, J. Electroanal. Chem. 638 (2010) 173–177.
[39] G. Slaughter, T. Kulkarni, Fabrication of palladium nanowire array electrode for biofuel cell application, Microelectron. Eng. 149 (2016) 92–96.
[40] G. Slaughter, T. Kulkarni, Detection of human plasma glucose using a self-powered glucose biosensor, Energies 12 (2019) 1–10.
[41] T. Matsumoto, A. Ohashi, N. Ito, Development of a micro-planar Ag/AgCl quasi-reference electrode with long-term stability for an amperometric glucose sensor, Anal. Chim. Acta 462 (2002) 253–259.
[42] H.F. Cui, J.S. Ye, W.D. Zhang, C.M. Li, John H.T. Luong, F.S. Sheu, Selective and sensitive electrochemical detection of glucose in neutral solution using platinum–lead alloy nanoparticle/carbon nanotube nanocomposites, Anal. Chim. Acta 594 (2007) 175–183.
[43] F. Wen, Y. Dong, L. Feng, S. Wang, S. Zhang, X. Zhang, Horseradish peroxidase functionalized fluorescent gold nanoclusters for hydrogen peroxide sensing, Anal. Chem. 83 (4) (2011) 1193–1196.
[44] G. Slaughter, K. Amoah, Vertically aligned Pd nanowires for glucose oxidase bioanode, J. Biosens. Bioelectron. 3 (4) (2012) 1–4.
[45] S.K. Krishnan, O.A. De Fuentes, E. Prokhorov, J.G. Luna-Barcenas, Electrochemical detection of hydrogen peroxide and glucose based on chitosan stabilized silver nanowire modified electrodes, IEEE Sensors 2014, pp. 1–4.
[46] K. Barman, S. Jasimuddin, Non-enzymatic electrochemical sensing of glucose and hydrogen peroxide using a bis(acetylacetonato)oxovanadium(IV) complex modified gold electrode, RSC Adv. 6 (2016) 20800–20806.
[47] J. Liu, L. Lu, A. Li, J. Tang, S. Wang, S. Xu, L. Wang, Simultaneous detection of hydrogen peroxide and glucose in human serum with upconversion luminescence, Biosens. Bioelectron. 68 (2015) 204–209.
[48] T. Kulkarni, G. Slaughter, Application of semipermeable membranes in glucose biosensing, Membranes 6 (2016) 1–20.
[49] Z. Ghassemi, G. Slaughter, Biological fuel cells and membranes, Membranes 7 (2017) 1–12.